Journal of Solid State Chemistry 182 (2009) 1884–1888

Contents lists available at ScienceDirect

Journal of Solid State Chemistry

journal homepage: www.elsevier.com/locate/jssc

Crystal structure of $BaMg_2Si_2O_7$ and Eu^{2+} luminescence

Cheol-Hee Park [a,*], Yong-Nam Choi [b]

[a] LG Chem Research Park, Daejeon 305-380, Republic of Korea
[b] Neutron Science Division, Korea Atomic Energy Research Institute, Daejeon 305-353, Republic of Korea

ARTICLE INFO

Article history:
Received 9 February 2009
Received in revised form
28 April 2009
Accepted 2 May 2009
Available online 9 May 2009

Keywords:
Barium magnesium silicate
$BaMg_2Si_2O_7$
Crystal structure
Neutron diffraction data
Eu^{2+} luminescence

ABSTRACT

Crystal structure of $BaMg_2Si_2O_7$ was determined and refined by a combined powder X-ray and neutron Rietveld method (monoclinic, $C2/c$, no. 15, $Z=8$, $a=7.24553(8)$ Å, $b=12.71376(14)$ Å, $c=13.74813(15)$ Å, $\beta=90.2107(8)^\circ$, $V=1266.44(2)$ Å^3; $R_p/R_{wp}=3.38\%/4.77\%$). The structure contains a single crystallographic type of Ba atom coordinated to eight O atoms with C_1 (1) site symmetry. Under 325-nm excitation $Ba_{0.98}Eu_{0.02}Mg_2Si_2O_7$ exhibits an asymmetric emission band around 402 nm. The asymmetric shape of the emission band is likely associated with a small electron–phonon coupling in $BaMg_2Si_2O_7$. The integrated intensity of the emission band was observed to remain constant over the temperature range 4.2–300 K.

1. Introduction

Alkaline earth silicates have received considerable attention because of their capacity to be used as luminescent materials [1,2]. Klasens and co-workers investigated ultraviolet luminescence from the Pb-activated ternary system of BaO–MgO–SiO_2, identifying the composition of $BaMg_2Si_2O_7$ [3]. Barry investigated luminescence properties of Eu^{2+}- and Mn^{2+}-doped $BaMg_2Si_2O_7$, where an effective energy transfer from Eu^{2+} to Mn^{2+} was observed [4]. Recently Ye et al. reported persistent red luminescence in $BaMg_2Si_2O_7$:Mn^{2+}, Eu^{2+}, Dy^{3+} [5].

The luminescence of Mn^{2+}, Pb^{2+}, and Eu^{2+} is highly sensitive to its local structure [1,2,6], which stipulates the necessity of determining the correct structure of the host material. However, the crystal structure of $BaMg_2Si_2O_7$ is currently unknown. Klasens and co-workers suggested that $BaMg_2Si_2O_7$ is isomorphous to $BaZn_2Si_2O_7$ due to the similarity between X-ray powder diffraction patterns of $BaMg_2Si_2O_7$ and $BaZn_2Si_2O_7$ [3]. The phase transition of $BaZn_2Si_2O_7$ was reported by Segnit et al. in 1970 [7]; the crystal structures of the low and high temperature phases were reported by Lin and co-workers in 1999 [8]. In this study we describe the crystal structure of $BaMg_2Si_2O_7$ and luminescence properties of Eu^{2+}-doped $BaMg_2Si_2O_7$.

2. Experimental

Powder samples of $BaMg_2Si_2O_7$ and $Ba_{0.98}Eu_{0.02}Mg_2Si_2O_7$ were prepared by solid-state reaction from stoichiometric mixtures of $BaCO_3$ (99.95%, Alfa), Eu_2O_3 (99.99%, Alfa), MgO (99.99%, High Purity Chemicals), and SiO_2 (99.99%, 1–3 mm pieces, Cerac). Prior to use, pieces of SiO_2 were ground into fine powder in an alumina mortar and pestle. For undoped $BaMg_2Si_2O_7$, the mixture was pressed into pellets and heated at 1523 K for a total of 60 h in air with intermediate grinding and pressing. The powder of $Ba_{0.98}Eu_{0.02}Mg_2Si_2O_7$ was prepared by heating the stoichiometric mixture at 1373 K for 10 h in air followed by cooling and grinding, and then reheating at 1523 K for 10 h under flowing H_2(g) (4%)/N_2(g) (96%) for 10 h. Energy dispersive X-ray (EDX) analysis performed using a Hitachi S-3400NX system led to results consistent with the stated compositions.

The powder X-ray diffraction (XRD) data were collected at room temperature on a Bragg–Brentano diffractometer (Bruker-AXS Advance D8) with a Cu X-ray tube, a focusing primary Ge (111) monochromator ($\lambda=1.5406$ Å), and a position sensitive Väntec detector over an angular range of $10^\circ \le 2\theta \le 151^\circ$ with a step of 0.016671°, and a total measurement time duration of 45 h.

The neutron powder diffraction data were collected at room temperature in air by using the HRPD which is installed at the research reactor HANARO (30MW) in the Korea Atomic Energy Research Institute (KAERI). The HANARO HRPD system is equipped with a combination of collimators, $C_1/C_2/C_3=20'/30'/10'$ and a vertically focusing mosaic monochromator (Ge(331) crystals, $\lambda=1.8349$ Å). The data were collected over the 2θ range

* Corresponding author. Fax: +82 42 861 2057.
E-mail address: pmoka@lgchem.com (C.-H. Park).

0022-4596/$ - see front matter © 2009 Elsevier Inc. All rights reserved.
doi:10.1016/j.jssc.2009.05.002

of 10–160° with a step of 0.05° and a total measurement time of 3 h. The sample was approximately 11.5 g.

The structure determination and refinement were performed by using TOPAS software [9] and the indexing program TREOR90 [10].

Photoluminescence measurements were made with the 325 nm line of a He–Cd continuous-wave laser (Omnichrome 2074) for excitation and a charge-coupled detector (Hamamatsu, C7042) for detection. Variable-temperature spectra were recorded by the use of a cryostat (Letbold, REF-1052M-4k5W) in the temperature range of 4.2–300 K.

3. Results and discussion

3.1. Powder X-ray and neutron diffraction analysis

In order to determine the unit cell, 20–30 peak positions of the XRD pattern at low angles were first obtained by single peak profile fitting run in TOPAS. A monoclinic unit cell with $a = 7.2414$ Å, $b = 12.70468$ Å, $c = 13.7455$ Å, $\beta = 90.21°$ was readily obtained from 20 peaks by TREOR90. At this point, the Inorganic Crystal Structure Database (ICSD) search for compounds with similar atomic ratios and unit cell dimensions resulted in $BaCo_2Si_2O_7$ ($C2/c$, $a = 7.2131(6)$ Å, $b = 12.781(1)$ Å, $c = 13.762(1)$ Å, $\beta = 90.299(8)°$) [11,12]. When $BaCo_2Si_2O_7$ was used as a starting model for $BaMg_2Si_2O_7$, a good Rietveld profile fitting was obtained with $R_p/R_{wp} = 3.53\%/4.50\%$. However, the interatomic distance of Si1–O7 was 1.521 Å with the average Si1–O distance of 1.58 Å, which was much shorter than the expected values from the sum of ionic radii: d(Si–O) = 1.64 Å [13]. This suggests that atomic coordinates were only approximate. Therefore, neutron diffraction data were collected. Neutron scattering lengths for the O atom ($b_{c,O} = 5.803$), the Si atom ($b_{c,Si} = 4.149$), and the Mg atom ($b_{c,Mg} = 5.375$) are known to be comparable to that for the much heavier Ba ($b_{c,Ba} = 5.07$), providing a means to accurately position these light atoms. In a previous study, neutron diffraction data were crucial in revealing the crystal structure of $Ba_3MgSi_2O_8$, because its superstructure reflections were observed only in the neutron diffraction data [14].

A combined Rietveld refinement of the X-ray and neutron diffraction data resulted in reasonable Si–O interatomic distances of 1.593(3)–1.667(3) Å with the average distance of 1.63(3) Å ($R_p/R_{wp} = 3.43\%/5.03\%$ for X-ray data, 3.30%/4.32% for neutron data, and 3.38%/4.77% for the combined data set). The refinement parameters were scale factors, background, unit-cell parameters, peak-profile coefficients, atomic coordinates, and isotropic thermal parameters. The final profile fits are shown in Fig. 1, and powder refinement results are given in Table 1. The refined atomic and isotropic displacement parameters are given in Table 2, and the important bond distances and angles are listed in Table 3.

3.2. The crystal structure

The structure of $BaMg_2Si_2O_7$ contains a single crystallographic Ba site, three crystallographically different Mg sites, two different Si sites, and seven different O sites. It is composed of discrete $[Si_2O_7]$ units connected through Mg atoms, which are coordinated tetrahedrally by four oxygen atoms derived from the $[Si_2O_7]$ groups (Fig. 2). The MgO_4 distorted tetrahedra form one-dimensional chains along the unit cell c-axis with Mg3–O4–Mg1–O4–Mg3–O1–Mg2–O1–Mg3 linkage. The Mg3–O4–Mg1 and Mg3–O1–Mg2 angles are 113.07(14)° and 127.43(17)°, respectively. The site symmetry is C_2 (2) for Mg1 and Mg2; on the other hand, the symmetry is C_1 (1) for Mg3. The average Mg–O distances

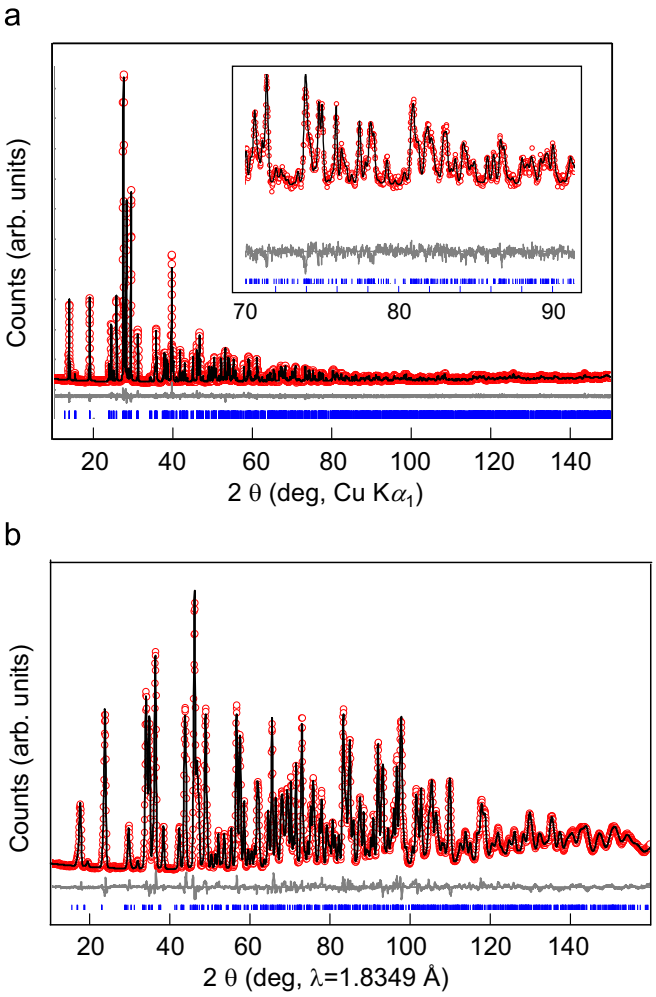

Fig. 1. Combined (a) X-ray ($\lambda = 1.5406$ Å) and (b) neutron ($\lambda = 1.8349$ Å) Rietveld refinement profiles for $BaMg_2Si_2O_7$ recorded at room temperature. The circle line marks experimental points and the solid line is the calculated profile. The lower trace shows the difference curve, and the ticks denote expected peak positions for $BaMg_2Si_2O_7$. The inset shows the high-angle data in detail.

Table 1
Results of structure refinement for $BaMg_2Si_2O_7$ from a combined powder X-ray and neutron diffraction data.

Chemical formula	$BaMg_2Si_2O_7$
Formula weight	2832.811
Space group	$C2/c$ (no. 15)
Z	8
a (Å)	7.24553(8)
b (Å)	12.71376(14)
c (Å)	13.74813(15)
β (deg)	90.2107(8)
V (Å^3)	1266.44(2)
d_{calc} (g/cm^3)	3.71435(7)
Temperature (K)	296
Number of reflections (X-ray/neutron)	1325/823
$R_p/R_{wp}/R_{exp}/R_B$ (X-ray) (%)[a]	3.43/5.03/1.56/2.94
$R_p/R_{wp}/R_{exp}/R_B$ (neutron) (%)[a]	3.30/4.32/1.20/1.87
R_p/R_{wp} (total) (%)[a]	3.38/4.77
Goodness of fit (total)	3.32
Total refined parameters	61

[a] $R_p = 100\Sigma|Y_{o,m}-Y_{c,m}|/\Sigma|Y_{o,m}|$; $R_{wp} = 100(\Sigma w_m|Y_{o,m}-Y_{c,m}|^2/\Sigma w_m|Y_{o,m}|^2)^{1/2}$; $R_B = 100(\Sigma|I_{o,k}-I_{c,k}|/\Sigma I_{o,k})$; $\chi^2 = 100\Sigma w|I_o-I_c|^2/(N_{obs}-N_{var})$; $R_{exp} = R_{wp}/|\chi|$.

are 1.953 Å for Mg1, 2.019 Å for Mg2, and 1.992 Å for Mg3. The discrete $[Si_2O_7]$ unit consists of vertex-sharing two distorted tetrahedra of $Si1O_4$ and Si_2O_4 with O5 as the bridging oxygen. The

Table 2
Atomic coordinates and isotropic displacement ($Å^2 \times 10^2$) for $BaMg_2Si_2O_7$ at room temperature.

Atom	Site	x	y	z	B_{iso} ($Å^2$)[a]
Ba	8*f*	0.20034(11)	0.01682(7)	0.12043(10)	0.55(2)
Mg1	4*e*	1/2	0.2693(3)	1/4	0.50(3)
Mg2	4*e*	1/2	0.7283(3)	1/4	0.50(3)
Mg3	8*f*	0.0364(3)	0.2352(2)	0.5083(2)	0.50(3)
Si1	8*f*	0.2842(3)	0.8740(2)	0.3666(2)	0.29(3)
Si2	8*f*	0.3211(3)	0.1052(2)	0.3792(3)	0.29(3)
O1	8*f*	0.4251(3)	0.7756(2)	0.3865(2)	0.73(2)
O2	8*f*	0.1720(3)	0.1156(2)	0.2943(2)	0.73(2)
O3	8*f*	0.2487(3)	0.1394(2)	0.4851(2)	0.73(2)
O4	8*f*	0.5018(8)	0.1812(2)	0.3662(2)	0.73(2)
O5	8*f*	0.4076(3)	−0.0160(2)	0.3776(3)	0.73(2)
O6	8*f*	0.2190(3)	0.8588(2)	0.2551(2)	0.73(2)
O7	8*f*	0.1170(3)	0.8840(2)	0.4411(2)	0.73(2)

[a] Constraints were placed on the atomic displacement factors for Mg1 = Mg2 = Mg3; Si1 = Si2; O1 = O2 = O3 = O4 = O5 = O6 = O7.

Table 3
Interatomic distances (Å) and selected angles (deg) in $BaMg_2Si_2O_7$ at room temperature.

Ba–O2	2.708(3)	O2–Ba–O2′	55.14(7)
Ba–O2′	3.202(3)	O2–Ba–O3	160.73(8)
Ba–O3	2.744(3)	O2–Ba–O4	71.40(6)
Ba–O4	3.010(2)	O2–Ba–O5	97.88(8)
Ba–O5	2.871(2)	O2–Ba–O6	75.33(9)
Ba–O6	2.736(3)	O2–Ba–O7	123.04(7)
Ba–O7	2.832(3)	O2–Ba–O7′	116.96(7)
Ba–O7′	2.973(3)	O2′–Ba–O3	129.93(8)
Mg1–O4 × 2	1.951(4)	O2′–Ba–O5	152.68(7)
Mg1–O6 × 2	1.954(3)	O2′–Ba–O6	94.58(7)
Mg2–O1 × 2	1.993(3)	O4–Mg1–O4′	109.97(11)
Mg2–O2 × 2	2.045(3)	O4–Mg1–O6	107.56(10)
Mg3–O1	1.926(3)	O4–Mg1–O6′	111.50(10)
Mg3–O3	1.989(4)	O6–Mg1–O6′	108.79(9)
Mg3–O4	2.046(4)	O1–Mg2–O1	145.85(11)
Mg3–O7	2.005(4)	O1–Mg2–O2	108.89(9)
Si1–O1	1.637(3)	O1–Mg2–O2′	95.66(9)
Si1–O5	1.667(3)	O2–Mg2–O2′	88.02(10)
Si1–O6	1.613(4)	O1–Mg3–O3	110.21(15)
Si1–O7	1.595(3)	O1–Mg3–O4	122.49(17)
Si2–O2	1.593(3)	O1–Mg3–O7	105.80(16)
Si2–O3	1.609(4)	O3–Mg3–O4	124.09(16)
Si2–O4	1.637(3)	O3–Mg3–O7	91.32(14)
Si2–O5	1.664(2)	O4–Mg3–O7	91.34(15)

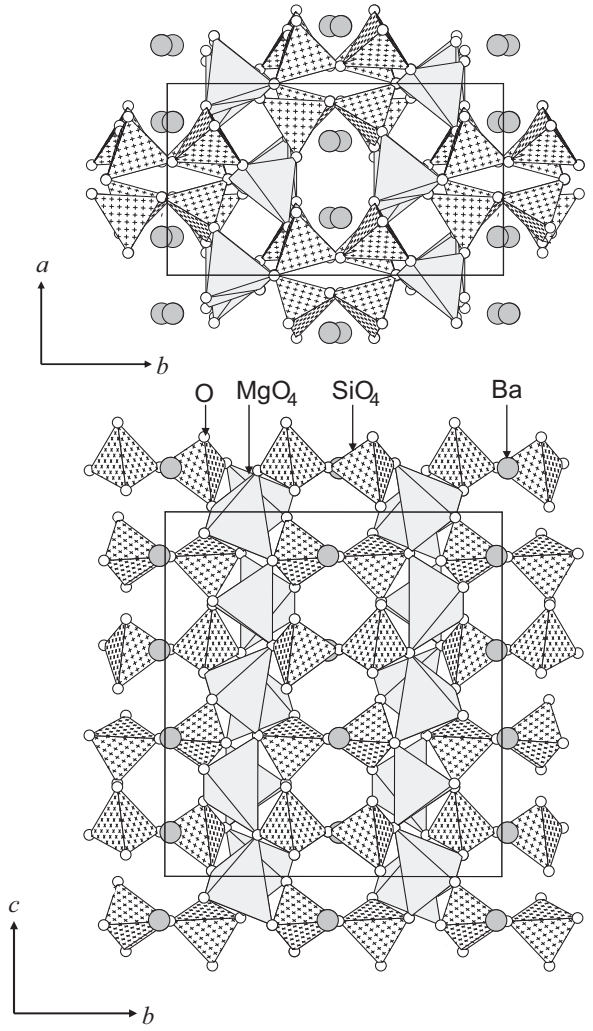

Fig. 2. Crystal structure of $BaMg_2Si_2O_7$ projected onto the *ab* plane (top) and the *bc* plane (bottom).

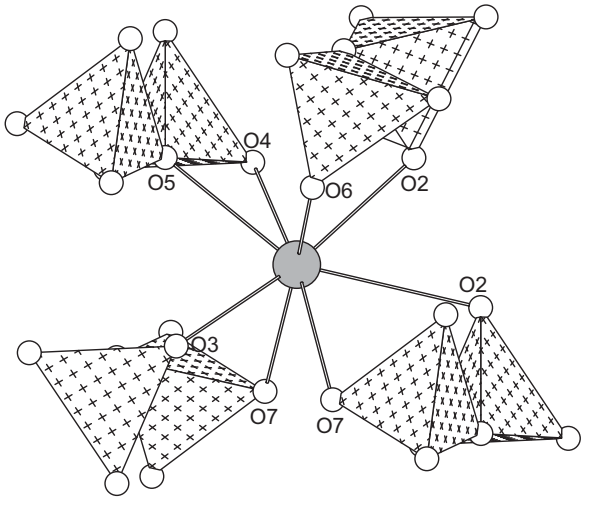

Fig. 3. The coordination environment of Ba atom. The Ba atom is coordinated to one bridging O5 atom and seven terminal O atoms of $[Si_2O_7]$ groups.

average Si–O distance is 1.63 Å with Si–O5 bridging distances (average 1.667 Å) longer than Si–O terminal distances (average 1.614 Å). The Si1–O5–Si2 angle in the $[Si_2O_7]$ group is 125.20(17)°, which is smaller than the Si–O–Si angle of the $[Si_2O_7]$ group observed in numerous compounds including the akermanite type $M_2MgSi_2O_7$ with the space group $P\bar{4}2_1m$ (144.3(5)° for M = Ba [15], 142.24° for M = Sr [16], 140.46° for M = Ca [17]) and pyrosilicates $M_2Si_2O_7$ (180° for M = Sc and Yb, 156° for Ln = Gd, and 133° for Nd [18]).

The Ba atom is coordinated to two O2, one O3, one O4, one O5, one O6, and two O7 atoms at distances of 2.708(3)–3.202(3) Å with the average length of 2.88(17) Å, which compares well to the value 2.80 Å computed from empirically derived radii [13]. The O environment about the Ba atom is depicted in Fig. 3. The symmetry of the Ba site is C_1 (1). The BaO_8 polyhedron shares one edge with one Si_2O_4 tetrahedron and six corners with six SiO_4 tetrahedra. The bond distance from the Ba atom to the bridging O5 atom of the $[Si_2O_7]$ group is 2.871(2) Å, which is close to the average Ba–O distance. The BaO_8 polyhedron distortion in $BaMg_2Si_2O_7$ is larger than those of polymorphic $Ba_2MgSi_2O_7$, which contain only one crystallographic type of Ba atoms coordinated to eight O atoms like $BaMg_2Si_2O_7$. The distortions of

the BaO_8 polyhedra are calculated as 30.1 for $BaMg_2Si_2O_7$, 10.4 for $Ba_2MgSi_2O_7$ with the space group $P\bar{4}2_1m$ [15], and 6.3 for $Ba_2MgSi_2O_7$ with the space group $C2/c$ [19] by using the equation proposed by Shimizu et al. [15]

$$D = \frac{1}{8} \times \sum \left(\frac{(Ri - R)}{R} \right)^2 \times 10^4,$$

where D is the distortion of the BaO_8 polyhedra, Ri is an individual bond length, and R is an average bond length.

The empirical expression for bond valence, which has been widely adopted to estimate valences in inorganic solids, was used to check the $BaMg_2Si_2O_7$ crystal structure. The bond valence sums [20] were calculated by using the software Valence [21]. The results are as follows: 1.72 (for Ba), 1.98 (Mg1), 1.66 (Mg2), 1.80 (Mg3), 3.97 (Si1), 3.99 (Si2), 1.94 (O1), 1.87 (O2), 1.78 (O3), 1.99 (O4, O5), 1.87 (O6), and 1.90 (O7). These values generally match the expected charges of the ions reasonably well. It is noteworthy that the calculated density (3.71 g/cm^3) of $BaMg_2Si_2O_7$ compares well with the average density (3.62 g/cm^3) of $BaMgSiO_4$ (4.02 g/cm^3) [22] and $MgSiO_3$ (3.21 g/cm^3) [23].

3.3. Luminescence

The emission spectrum of the $Ba_{0.98}Eu_{0.02}Mg_2Si_2O_7$ powder ($\lambda_{exc} = 325$ nm) measured at 300 K reveals a broad band around 402 nm (3.08 eV) with a full width at half-maximum (FWHM) of 26 nm (Fig. 4), which agrees well with observations in $Ba_{0.96}Eu_{0.04}Mg_2Si_2O_7$ by Barry [4]. The emission band appears to be asymmetric on an energy scale. The excitation band with the lowest energy of $Ba_{0.96}Eu_{0.04}Mg_2Si_2O_7$ is reported to be observed around 380 nm [4,24], which is higher in energy than that of $Ba_2MgSi_2O_7$:Eu^{2+} (450 nm) [24]. The energy of the $4f^7 \rightarrow 4f^6 5d^1$ excitation band is sensitive to the crystal field at Eu^{2+} site. The average Ba–O distances are 2.88 Å for $BaMg_2Si_2O_7$ and 2.80 Å for $Ba_2MgSi_2O_7$ [15]. The smaller Ba–O distance will result in higher crystal field and will decrease the energy of the excitation band of $Ba_2MgSi_2O_7$:Eu^{2+}. The energy of the excitation band is also affected by bond covalency (or nephelauxetic effect), which is mainly affected by the local nearest-neighbor and the next nearest-neighbor interactions at the dopant site. The nearest-neighbor and the next nearest-neighbor interactions for Eu substituted on this site are predominantly characterized by Eu–O–Ba, Eu–O–Mg, and Eu–O–Si linkages. In $Ba_2MgSi_2O_7$:Eu^{2+} O atoms are linked to more Ba atoms, resulting in more Eu–O–Ba interactions than in $BaMg_2Si_2O_7$:Eu^{2+}. The more ionic nature of the Ba–O bond relative to the Mg–O and Si–O will depress the energy of the $4f^7 \rightarrow 4f^6 5d^1$ excitation band. A detailed discussion will be given elsewhere.

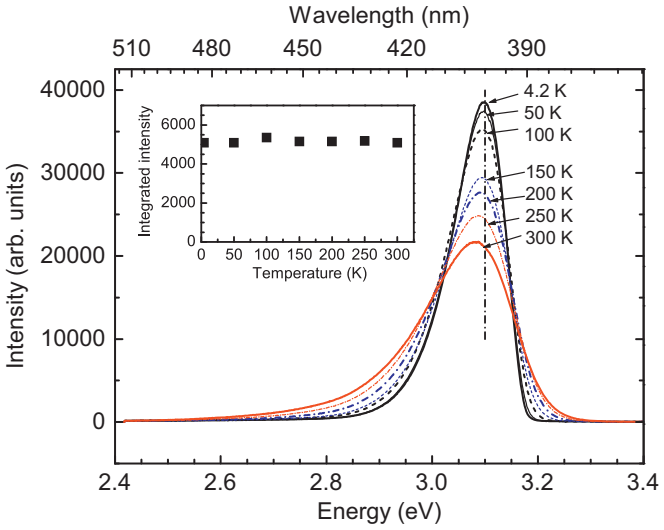

Fig. 4. Emission spectra of $Ba_{0.98}Eu_{0.02}Mg_2Si_2O_7$ measured at different temperatures from 4.2 to 300 K under excitation at 325 nm. With increasing temperatures the maximum intensity of the emission band decreases and its FWHM increases. The inset shows the integrated intensity of the emission band as a function of the temperature.

The energetic position of the Eu^{2+} emission is strongly dependent on its local structure [1–2,6]. Van Uitert investigated emission from Eu^{2+} ions in various compounds and proposed an empirical relation [25]

$$E(\mathrm{cm}^{-1}) = Q \times [1 - (V/4)^{1/V} \times 10^{-(n \times ea \times r)/80}],$$

where E is the position in energy for the Eu^{2+} emission peak, Q is the position in energy for the lower d-band edge for the free Eu^{2+} ion ($Q = 34\,000\ \mathrm{cm}^{-1}$), V is the valence of the Eu^{2+} ion ($V = 2$), n is the number of anions in the immediate shell about the Eu^{2+} ion, ea is the electron affinity of the atoms that form anions (in eV), and r is the radius of the host cation replaced by the Eu^{2+} ion (in Å) [25]. By using values of ea for O (2.5 eV), coordination number of Ba atom in $BaMg_2Si_2O_7$ ($n = 8$), and $r = 1.66$ Å computed from the average Ba–O bond distance in $BaMg_2Si_2O_7$ and the Shannon radius of O^{2-} with coordination number of 3 (1.22 Å) [13], the equation provides the position of the emission peak of 403 nm (24 800 cm^{-1}), which is in good agreement with the observed value. It is worth to note that even though Van Uitert's empirical relation showed a good agreement in our case, the agreement for other materials may not be so relevant. For example, the emission peak position of $Ba_2MgSi_2O_7$:Eu^{2+} derived from the equation (410 nm) does not match closely to the observed value of 500 nm [24]. The position of the emission band is normally determined by various factors such as crystal field, bond covalency, Stokes shift, and preferred orientations of d orbitals [26,27].

Asymmetric band shape of Eu^{2+} emission is often associated with the presence of Eu^{2+} on multiple crystallographic sites [26–28]. However, there is only one crystallographic Ba site in $BaMg_2Si_2O_7$, and tetrahedrally coordinated Mg sites are too small to accommodate Eu^{2+}. Another rationale is a small electron–phonon coupling in $BaMg_2Si_2O_7$. It is known that the emission band shape becomes more asymmetric with decreasing electron–phonon coupling [29]. To determine the strength of the electron–phonon coupling, fit of the emission band measured at 4.2 K was performed. A broad emission band is composed of vibronic transitions, and the shape of the emission band can be obtained by calculating the intensity of each vibronic transition. At the temperature $T = 0$ K, only the fundamental vibrational level of the excited state is occupied, and the intensity of each vibronic transition ($m = 0 \rightarrow n$) is proportional to the relation [29]

$$\frac{\exp(-S) \times S^n}{n!},$$

where S is the Huang–Rhys parameter which is a measure of the strength of the electron–phonon interaction. The energy gap between two vibronic states is equal to the quantity $h\nu$, the mean phonon energy for the $4f^7$ ground state. A reasonable fit of the emission band was carried out with $S = 2.5$ and $h\nu = 35.5$ meV (Fig. 5). This S value corresponds to an intermediate electron–phonon coupling, and results in asymmetric emission band [1,29]. If the excited-state and ground-state parabolas on configurational coordinate model are identical, the Stokes shift, i.e. the energy difference between the emission band and the absorption band peaks, has a magnitude $(2S-1)h\nu$. By using the above S and $h\nu$ the Stokes shift of $Ba_{0.98}Eu_{0.02}Mg_2Si_2O_7$ is calculated as 1145 cm^{-1} [29]. It is worth noting that the

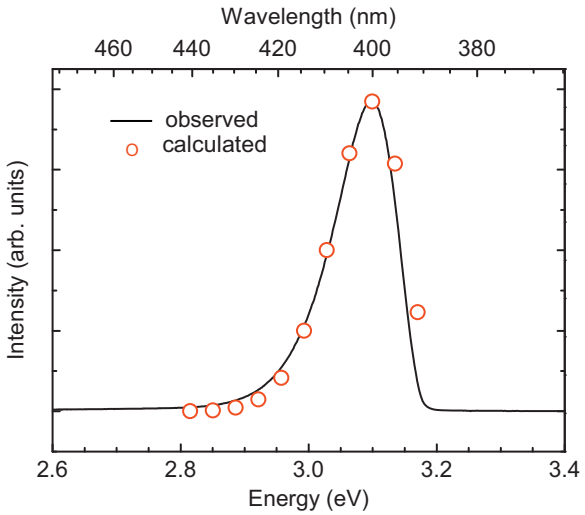

Fig. 5. Observed (solid line) and calculated (open circle) emission spectrum of $Ba_{0.98}Eu_{0.02}Mg_2Si_2O_7$ recorded at 4.2 K under excitation at 325 nm.

reported Stokes value of $Ba_{0.96}Eu_{0.04}Mg_2Si_2O_7$ at room temperature is 1316 cm^{-1} [4,24].

When the temperature was decreased from 300 to 4.2 K, the emission band of $Ba_{0.98}Eu_{0.02}Mg_2Si_2O_7$ slightly shifts from 402 to 400 nm (Fig. 4), which may be associated with the decrease in the energy for the most occupied vibrational level of the $4f^65d^1$ excited electronic state [29]. No additional emission band is observed over the range 360–700 nm with decreasing temperature. It is also observed that as the temperature decreases the maximum intensity of the emission band increases and its FWHM decreases, which is related to the decrease in thermal occupancy in high-order vibrational states [29].

The maximum intensity of the emission band of $Ba_{0.98}Eu_{0.02}Mg_2Si_2O_7$ measured at 300 K drops to 56% of the maximum intensity at 4.2 K, which is similar to observation in $BaMgSiO_4:Eu^{2+}$; its maximum intensity of the emission band at 300 K falls to the half of the maximum intensity at 4.2 K [27]. The integrated intensity of the emission band of $Ba_{0.98}Eu_{0.02}Mg_2Si_2O_7$, however, does not change in the temperature range of 4.2–300 K (Fig. 4). For a number of silicates, temperature dependency of the maximum intensity of the emission band is reported, whereas reports on temperature dependency of the integrated intensity are rare [24]. Chartier et al. observed that in $SrGa_2S_4:Eu^{2+}$ the integrated PL intensity and the decay time of the luminescence are constant in the temperature range of 77–350 K [30]. The luminescent decay is represented by an exponential curve in the temperature range. From 350 K both of the integrated PL intensity and the decay time decrease with increasing temperature. These observations imply that non-radiative decay processes are important only beyond 350 K. Similarly in $Ba_{0.98}Eu_{0.02}Mg_2Si_2O_7$ non-radiative decay processes might be negligible in the temperature range of 4.2–300 K.

4. Conclusions

The previously unconfirmed crystal structure of $BaMg_2Si_2O_7$ was determined and refined with a combined Rietveld refinement of powder X-ray and neutron diffraction data. The structure contains a single crystallographic type of Ba atom coordinated to eight O atoms with C_1 (1) site symmetry. Under 325-nm excitation at room temperature, $Ba_{0.98}Eu_{0.02}Mg_2Si_2O_7$ exhibits an emission band with maximum at 402 nm, which agrees well with the calculated value by using Van Uitert's empirical equation and the crystallographic information obtained in this study. The maximum intensity of the emission band decreases by 44% with increasing temperature from 4.2 to 300 K. However, the integrated intensity of the emission band does not change in the temperature range.

Supporting information

Further details of the crystal structure may be obtained from the Fachinformationszentrum Karlsruhe, D-76344 Eggenstein-Leopoldshafen, Germany (fax: +49 7247 808 666; e-mail: crysdata@fiz-karlsruhe.de) on quoting the depository number CSD-420258 for $BaMg_2Si_2O_7$.

Acknowledgment

The authors would like to thank Mr. B.J. Chae in LG Chem Research Park for the EDX analysis.

Appendix A. Supplementary material

Supplementary data associated with this article can be found in the online version at doi:10.1016/j.jssc.2009.05.002.

References

[1] S. Shionoya, W.M. Yen (Eds.), Phosphor Handbook, CRC Press, Boca Raton, 2000.
[2] G. Blasse, B.C. Grabmaier, Luminescent Materials, Springer, Berlin, 1994.
[3] H.A. Klasens, A.H. Hoekstra, A.P.M. Cox, J. Electrochem. Soc. 104 (2) (1957) 93–100.
[4] T.L. Barry, J. Electrochem. Soc. 117 (3) (1970) 381–385.
[5] S. Ye, J. Zhang, X. Zhang, X. Wang, J. Lumin. 122–123 (2007) 914–916.
[6] G. Blasse, A. Bril, Philips Tech. Rev. 31 (1970) 304–334.
[7] E.R. Segnit, A.E. Holland, Aust. J. Chem. 23 (1970) 1077–1085.
[8] J.H. Lin, G.X. Lu, J. Du, M.Z. Su, C.-K. Loong, J.W. Richardson Jr, J. Phys. Chem. Solids 60 (1999) 975–983.
[9] R.W. Cheary, A. Coelho, J. Appl. Crystallogr. 25 (1992) 109–121
Bruker AXS, TOPAS 3, Karlsruhe, Germany, 2000.
[10] P.E. Werner, L. Eriksson, M. Westdahl, J. Appl. Crystallogr. 18 (1985) 367–370.
[11] ICSD (Inorganic Crystal Structure Database), v. 2005-1, Karlsruhe, Germany, 2005.
[12] R.D. Adams, R. Layland, C. Payen, T. Datta, Inorg. Chem. 35 (1996) 3492–3497.
[13] R.D. Shannon, Acta Crystallogr. A 32 (1976) 751–767.
[14] C.-H. Park, S.-T. Hong, D.A. Keszler, J. Solid State Chem. 182 (2009) 496–501.
[15] M. Shimizu, M. Kimata, I. Iida, N. Jb. Miner. Mh. H1 (1995) 39–47 (ICSD #81117).
[16] M. Kimata, Z. Kristallogr. 163 (1983) 295–304 (ICSD #31308).
[17] I.P. Swainson, M.T. Dove, W.W. Schmahl, A. Putnis, Phys. Chem. Miner. 19 (1992) 185–195 (ICSD #67692).
[18] A.F. Wells, Structural Inorganic Chemistry, fifth ed., Oxford University Press, New York, 1984, p. 1019.
[19] T. Aitasalo, J. Hölsä, T. Laamanen, M. Lastusaari, L. Lehto, J. Niittykoski, F. Pellé, Z. Kristallogr., (Suppl. 23) (2006) 481–486.
[20] I.D. Brown, D. Altermatt, Acta Crystallogr. B 41 (1985) 244–247.
[21] N.E. Brese, M. O'Keeffe, Acta Crystallogr. B 47 (1991) 192–197.
[22] B. Liu, J. Barbier, J. Solid State Chem. 102 (1993) 115–125.
[23] N. Morimoto, K. Koto, Z. Kristallogr. 129 (1969) 65–83.
[24] P. Dorenbos, J. Lumin. 104 (2003) 239–260.
[25] L.G. Van Uitert, J. Lumin. 29 (1984) 1–9.
[26] A. Diaz, D.A. Keszler, Chem. Mater. 9 (1997) 2071–2077.
[27] S.H.M. Poort, H.M. Reijnhoudt, H.O.T. Van der Kuip, G. Blasse, J. Alloys Compd. 241 (1996) 75–81.
[28] S.H.M. Poort, W.P. Blokpoel, G. Blasse, Chem. Mater. 7 (1995) 1547–1551.
[29] B. Henderson, G.F. Imbusch (Eds.), Optical Spectroscopy of Inorganic Solids, Clarendon Press, Oxford, 1989.
[30] C. Chartier, C. Barthou, P. Benalloul, J.M. Frigerio, J. Lumin. 111 (2005) 147–158.